Hindawi Publishing Corporation
EURASIP Journal on Wireless Communications and Networking
Volume 2007, Article ID 32807, 9 pages
doi:10.1155/2007/32807

Research Article

Direct Conversion EHM Transceivers Design for Millimeter-Wave Wireless Applications

Abbas Mohammadi,[1] Farnaz Shayegh,[2] Abdolali Abdipour,[1] and Rashid Mirzavand[1]

[1] *Microwave and Wireless Communication Research Labratory, Electrical Engineering Department, Amirkabir University of Technology (Polytechnic), Tehran 1587-4413, Iran*
[2] *Electrical and Computer Engineering Department, Concordia University, Montreal, QC, Canada H4G2W1*

Received 29 March 2006; Revised 14 November 2006; Accepted 15 November 2006

Recommended by Kiyoshi Hamaguchi

A direct conversion modulator-demodulator with even harmonic mixers for fixed wireless applications is presented. The circuits consist of even harmonic mixers (EHMs) realized with antiparallel diode pairs (APDPs). A communication link is set up to examine the overall performance of proposed modulator-demodulator. The transmission of 16-QAM signal with 110 Mbps data rate over fixed wireless link has been examined. We also evaluate the different levels of I/Q imbalances and DC offsets and use signal space concepts to analyze the bit error rate (BER) of the proposed transceiver using M-ary QAM schemes. The results show that this structure can be efficiently used for fixed wireless applications in Ka band.

1. INTRODUCTION

Local multipoint distribution system (LMDS) is a broadband wireless point-to-multipoint communication system operating above 20 GHz and provide high-data-rate voice, TV, and internet services. It is desirable to increase the spectral efficiency or the transmission capacity of LMDS services by using sophisticated amplitude and phase modulation techniques (QPSK and QAM). The cost reduction in LMDS transceiver design is a key issue to increase the deployment of this system. Among various realization techniques, the direct conversion implementation reduces the size and cost of LMDS transceiver. A direct conversion modulator-demodulator using even harmonic mixers (EHMs) is designed at 28 GHz for LMDS applications. The EHM is based on antiparallel diode pair (APDP). The APDP has a balanced structure that suppresses the fundamental mixing products ($mf_{LO} \pm nf_{IF}$ where $m + n =$ even). These products flow only within the APDP loop [1]. The EHM with APDP has some advantages that make it very attractive for millimeter-wave transceivers. These advantages are: (1) it can operate with halved LO frequency; (2) in direct conversion transmitter, it can suppress the virtual LO leakage ($2f_{LO}$) that locates nearby a desired RF signal; (3) it suppresses DC offset in direct conversion receivers.

The paper is organized as follows: the even harmonic mixer structure and three methods to improve its behavior are introduced. Then, a direct conversion modulator is designed using even harmonic mixers. The modulator structure is reciprocal and can also be used as a direct conversion demodulator. Next, we consider the effects of I/Q imbalances and DC offsets on the bit-error-rate performance of the demodulator for M-ary QAM schemes. Finally, a communications link using direct 16-QAM modulator-demodulator with 110 Mbps data rate is successfully demonstrated.

2. EVEN HARMONIC MIXER

Figure 1(a) shows a circuit configuration of the even harmonic mixer (EHM). It includes open-and short-circuited stubs at each port of the APDP. Both of them have a quarter-wave length at LO frequency. Using these stubs, the BPF and the LPF, the leakage of each port at other ports is suppressed [2]. The BPF is designed to cover the RF band of 27.5-28.5 GHz. It is a third-order chebycheve filter with center frequency of 28 GHz. The filter insertion loss (S12) and also the filter S11 curves in dB are shown in Figure 2. As we can see from the filter insertion loss, the filter center frequency is 28 GHz and its 3-dB bandwidth is 1 GHz from 27.5 GHz to 28.5 GHz. In 28 GHz, the amount of S11 and S22 in dB is

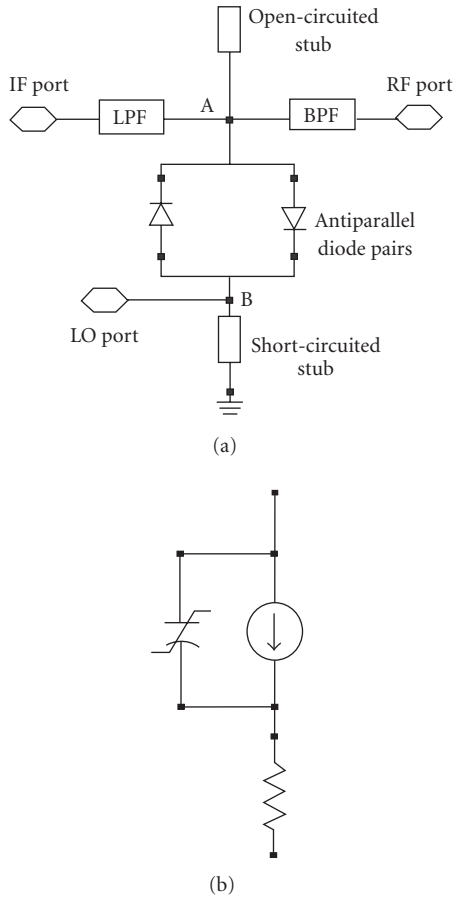

Figure 1: (a) Circuit configuration of the even harmonic mixer, (b) Schottky diode nonlinear model.

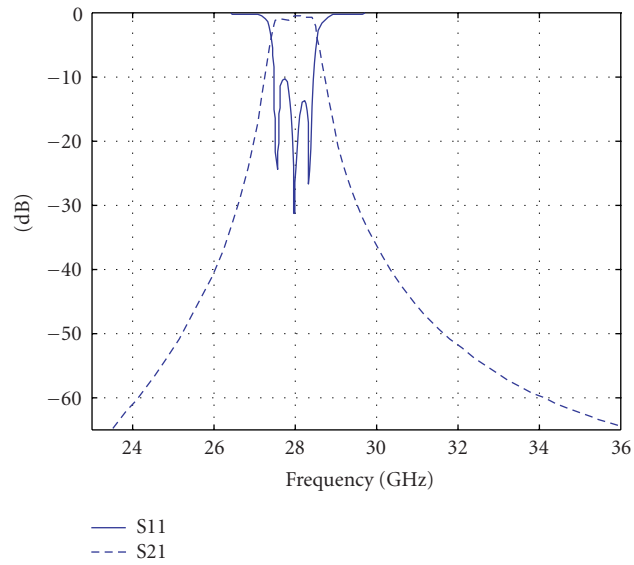

Figure 2: Filters S11 and S12 (dB).

Table 1: Diode parameters.

Junction capacitance (Cj0)	0.04 pF
Series resistance (Rs)	6 Ω
Saturation current (Is)	1.6E-13A
Ideality factor (N)	1.2

−28.674, so there is a good matching in filter input and output. The GaAs Schottky barrier APDP (agilent HSCH-9551) is used to realize the mixer. Table 1 shows its parameters.

This mixer is used to mix the baseband signal (at 100 MHz) with the second harmonic of the LO signal (at 13.95 GHz) to provide the RF signal at 28 GHz. Figure 3 shows the mixer conversion gain versus LO power [3]. This results are obtained from the harmonic-balance simulation. Figure 1(b) shows the Schottky diode nonlinear model. In continue, we introduce three ways to improve the mixer behavior and reduce its conversion loss.

2.1. Matching networks

In this section, matching networks in both sides of the APDP are included in an effort to reduce the mixer conversion loss and the LO power required for optimal mixer conversion loss [4]. LO matching network consists of a series delay line followed by a shunt short-circuited stub. RF matching network consists of a series delay line followed by a shunt open-circuited stub. These matching networks are designed to match the APDP impedance at the LO and RF ports to 50 ohm. The length of these stubs is iteratively tuned to provide good conversion loss at a relatively low LO drive level. Figure 4 shows the mixer conversion gain versus LO power with and without the matching networks. As we can see from this figure, matching networks result in decrease of LO power required for optimal mixer conversion loss and a slight improvement in mixer conversion loss.

2.2. Parallel diodes

As we know, series resistance (Rs) of Schottky diodes is a major factor in diode mixer conversion loss. If two parallel Schottky diodes are substituted for each diode in APDP, effective Rs of the structure will be divided by an approximate factor of two and the conversion loss will be decreased [5]. Also use of three diodes instead of each diode causes more decrease in mixer conversion loss. For each of the above cases, matching networks should be designed again.

Figure 5 shows the mixer conversion loss with one, two, and three diodes.

2.3. Self-biased APDP

Another way to improve the conversion loss of our mixer is to use self-biased APDP [6]. In this case, RC networks in both sides of each diode are designed to flatten the conversion loss of the even harmonic mixer. The values of RC networks are R = 150 ohm, C = 50 pf. Figure 6 shows conversion gain versus LO power with self-biased APDP and conventional

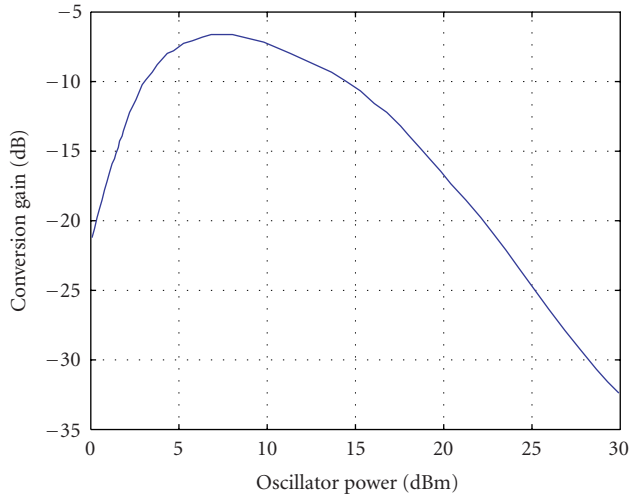

Figure 3: Conversion gain of the EHM.

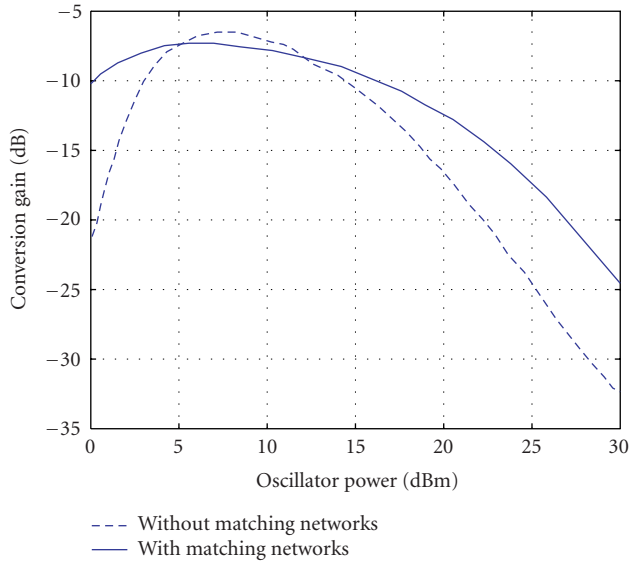

Figure 4: Mixer conversion gain.

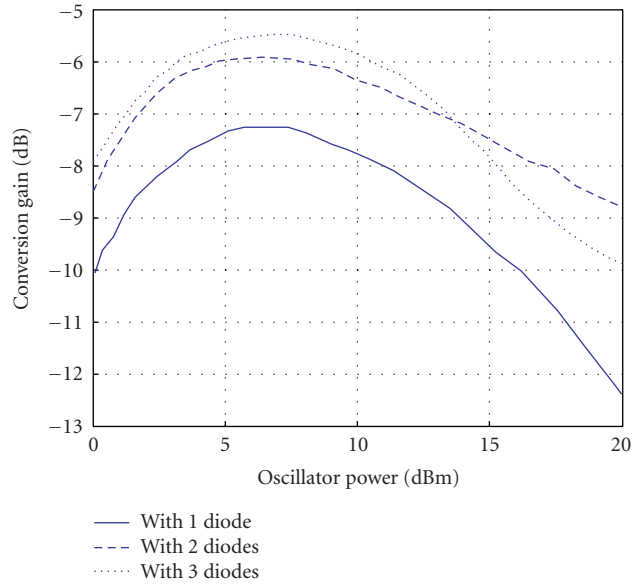

Figure 5: Mixer conversion gain.

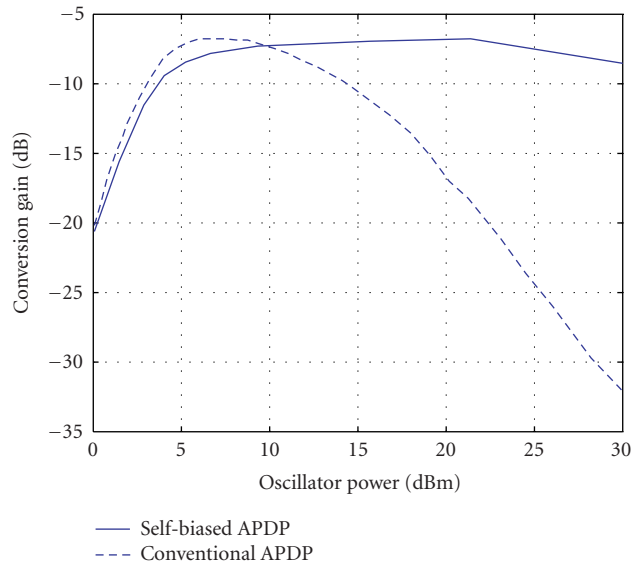

Figure 6: Conversion gain of the EHM using self-biased APDP and conventional APDP.

APDP. The conversion loss of EHM using self-biased APDP is almost constant from 10 dBm to 25 dBm of LO power.

2.3.1. Numerical results

We also write a program with Matlab software in order to calculate the conversion loss of the EHM using self-biased APDP by the harmonic-balance method. Diode parameters used for calculation are obtained from the agilent HSCH-9551 data sheet. We set the RF frequency to 28 GHz and the RF power to −75 dBm. The RF signal is mixed with second harmonic of the LO signal. Figure 7 shows calculated conversion gain versus LO power. As may be seen, the calculated results agree well with the simulated results. In order to have the best mixer behavior, self-biased APDP is used and three diodes are substituted for each diode in APDP. In addition to this, matching networks are designed in both sides of the APDP. Figure 8 shows the mixer structure used in our design. In continue, we consider the third-order intermodulation results [7]. To do this, two sinusoidal signals at the same amplitude and little frequency difference (28.007 GHz, 27.93 GHz) are inserted at the RF port and input and output IP3 (third-order intercept point) are calculated. Figure 9 shows the results.

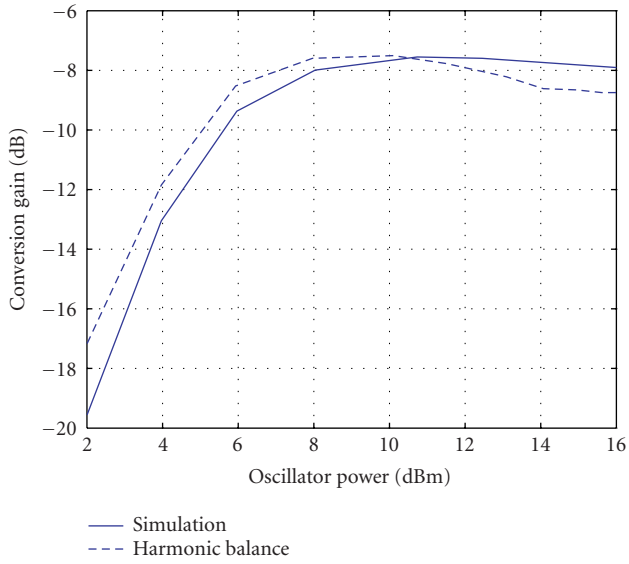

FIGURE 7: Conversion gain of the EHM using self-biased APDP calculated by the harmonic balance method and compared with simulated results.

3. MODULATOR STRUCTURE

The proposed I-Q modulator consists of two even harmonic mixers as shown in Figure 10. The LO signal is splited by a Wilkinson power divider, and a 45° delay line is connected to one of Wilkinson power divider arms to provide 90° phase difference at the second harmonic of the LO [8]. The LO carriers are mixed with baseband modulating signals (I and Q) in even harmonic mixers. Finally, both mixed signals are combined in a Wilkinson power combiner and the modulated signal is produced.

The following formulas illustrate the modulator inputs:

$$\begin{aligned} v_{\mathrm{LO}}(t) &= \cos \omega_{\mathrm{LO}} t, \\ v_I(t) &= \cos \omega_{\mathrm{IF}} t, \\ v_Q(t) &= \cos\left(\omega_{\mathrm{IF}} t + 90\right). \end{aligned} \tag{1}$$

Then, the outputs of EHMs can be obtained as follows:

$$\begin{aligned} e_1(t) &= \cos 2\omega_{\mathrm{LO}} t \times \cos \omega_{\mathrm{IF}} t, \\ e_2(t) &= \cos\left(2\omega_{\mathrm{LO}} t - 90\right) \times \cos\left(\omega_{\mathrm{IF}} t + 90\right). \end{aligned} \tag{2}$$

Finally, using Wilkinson power combiner, the modulated signal is as follows:

$$e(t) = e_1(t) + e_2(t) = \cos\left(2\omega_{\mathrm{LO}} + \omega_{\mathrm{IF}}\right) t. \tag{3}$$

As may be seen, the lower sideband component $(2f_{\mathrm{LO}} - f_{\mathrm{IF}})$ is suppressed without external filters.

In order to characterize the modulator performance, we insert two sinusoidal carriers at the same low frequency ($f_{\mathrm{IF}} = 100\,\mathrm{MHz}$), same amplitude, and quadrature phase on the I and Q inputs. Figure 11 shows the RF spectrum of the modulator operating at LO power of 10 dBm and LO frequency of 13.95 GHz. The power of virtual LO leakage $(2f_{\mathrm{LO}} = 27.9\,\mathrm{GHz})$ is −67 dBm. So, the suppression of the virtual LO leakage of 77 dB is obtained. The lower sideband component $(2f_{\mathrm{LO}} - f_{\mathrm{IF}} = 27.8\,\mathrm{GHz})$ is 25 dB lower than the desired component $(f_{\mathrm{RF}} = 2f_{\mathrm{LO}} + f_{\mathrm{IF}} = 28\,\mathrm{GHz})$.

Figure 12 shows the conversion gain of the whole modulator using a self-biased APDP and a conventional APDP.

4. DEMODULATOR

As mentioned above, the modulator is realized with passive components and the mixer is based on Schottky diodes that do not need DC bias circuitry. Accordingly, the whole modulator has zero DC power consumption. This modulator is totally reciprocal and can be used as a demodulator [9]. To characterize this circuit as a demodulator, a sinusoidal signal is inserted on RF port and the power at I and Q outputs is measured. Figure 12 shows conversion gain of the demodulator versus RF frequency from 26 to 30 GHz. The figure shows that the demodulator has bandwidth better than 1.5 GHz. The average conversion loss is 7.5 dB around 28 GHz for both channels.

5. BER CALCULATIONS

In this section, we consider the impacts of I/Q imbalances and DC offsets on QAM detection in the demodulator. The input signal in the RF port is a QAM signal and can be written as follows:

$$X_{\mathrm{RF}}(t) = \sqrt{\frac{2E_{\min}}{T_s}}\left(a_i \cos\left(2\pi f_c t\right) + b_i \sin\left(2\pi f_c t\right)\right), \tag{4}$$

where

$$\{a_i, b_i\} = \begin{bmatrix} (-L+1, L-1)(-L+3, L-1)\cdots(L-1, L-1) \\ (-L+1, L-3)(-L+3, L-3)\cdots(L-1, L-3) \\ \vdots \\ (-L+1, -L+1)(-L+3, -L+1)\cdots(L-1, -L+1) \end{bmatrix}, \quad i = 1, 2, \ldots, L;\ L = \sqrt{M}. \tag{5}$$

M is restricted to 2^P so that each symbol can be represented by P bits. We will restrict our consideration to Gray code bit mapping [10]. The Gray code mapping has the property that two P-bit symbols corresponding to adjacent symbols differ in only a single bit. As a result, an error in an adjacent symbol is accompanied by one and only one bit error. Finally, we do our calculations under AWGN channel.

5.1. BER calculations in presence of I/Q imbalances

We assume that the I and Q paths of LO signal in the demodulator are equal to

$$\begin{aligned} X_{\mathrm{Lo},I}(t) &= \left(1 + \frac{\varepsilon}{2}\right) \cos\left(\omega_{\mathrm{Lo}} t + \frac{\theta}{2}\right), \\ X_{\mathrm{Lo},Q}(t) &= \left(1 - \frac{\varepsilon}{2}\right) \cos\left(\omega_{\mathrm{Lo}} t - \frac{\theta}{2}\right), \end{aligned} \tag{6}$$

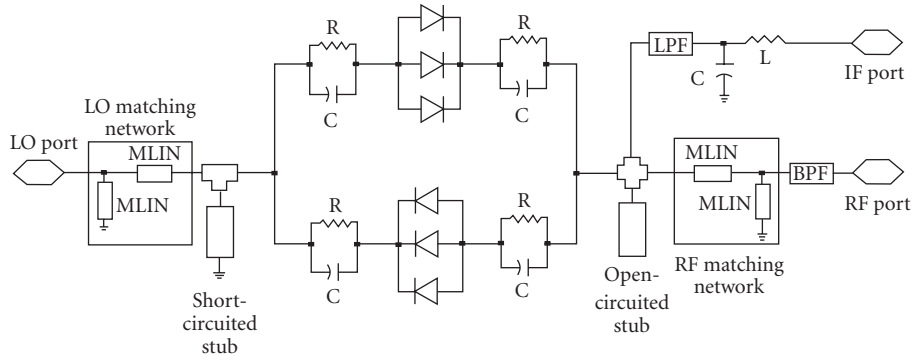

Figure 8: EHM structure used in our design.

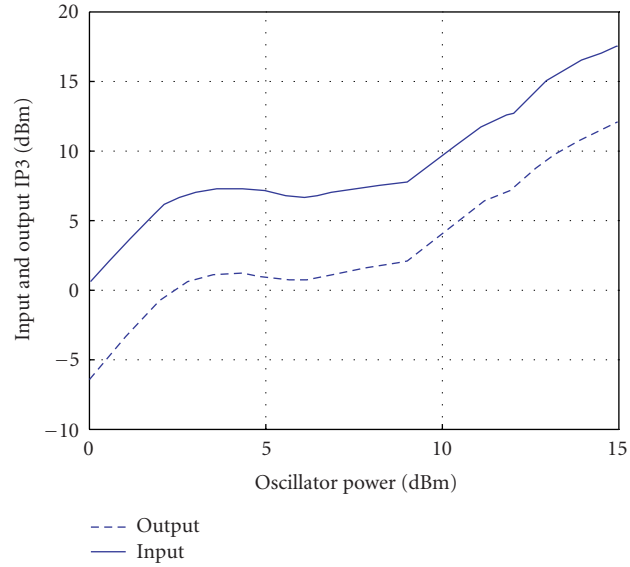

Figure 9: Input and output IP3 versus LO power for self-biased EHM.

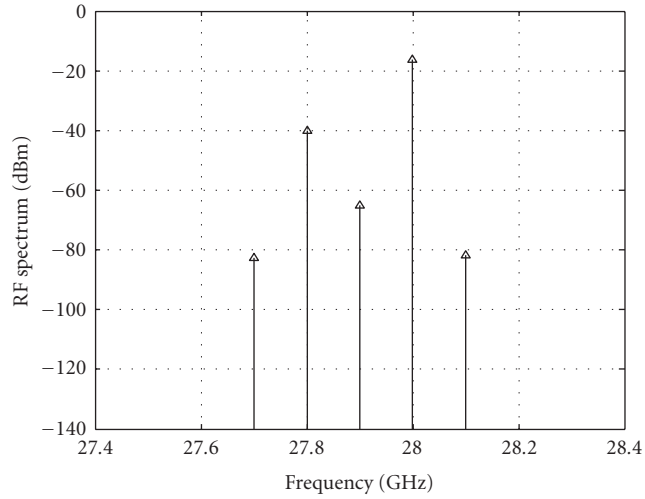

Figure 11: Spectrum at output of the modulator.

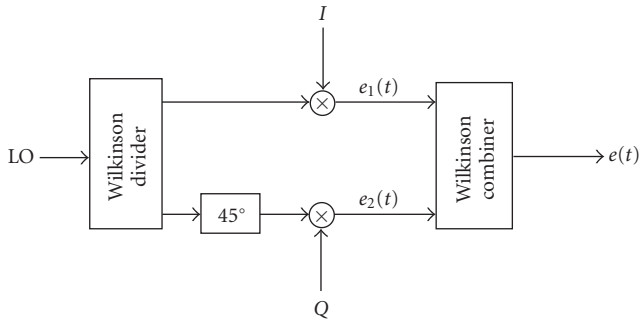

Figure 10: Modulator scheme.

where ε and θ represent gain and phase errors, respectively. As we know from [1], the conductance expression for an APDP can be written as follows:

$$g = 2\alpha i_s \cosh(\alpha V). \tag{7}$$

In this formula, α and i_s are the slope ($\alpha = q/kT$) and saturation current of diodes. For the usual case in which only the LO signal modulates the conductance of the diodes, we may substitute $V = X_{\mathrm{Lo}}(t)$. So, conductances in I and Q paths may be expanded in the following series [1]:

$$\begin{aligned} g_I &= 2\alpha i_s \left[I_0\left(\alpha\left(1+\frac{\varepsilon}{2}\right)\right) \right. \\ &\qquad \left. + 2I_2\left(\alpha\left(1+\frac{\varepsilon}{2}\right)\right)\cos\left(2\omega_{\mathrm{Lo}}t+\theta\right)+\cdots \right], \\ g_Q &= 2\alpha i_s \left[I_0\left(\alpha\left(1-\frac{\varepsilon}{2}\right)\right) \right. \\ &\qquad \left. + 2I_2\left(\alpha\left(1-\frac{\varepsilon}{2}\right)\right)\sin\left(2\omega_{\mathrm{Lo}}t-\theta\right)+\cdots \right], \end{aligned} \tag{8}$$

where I_n are modified Bessel functions of the first kind. So, the output currents in I and Q ports after a lowpass filter are

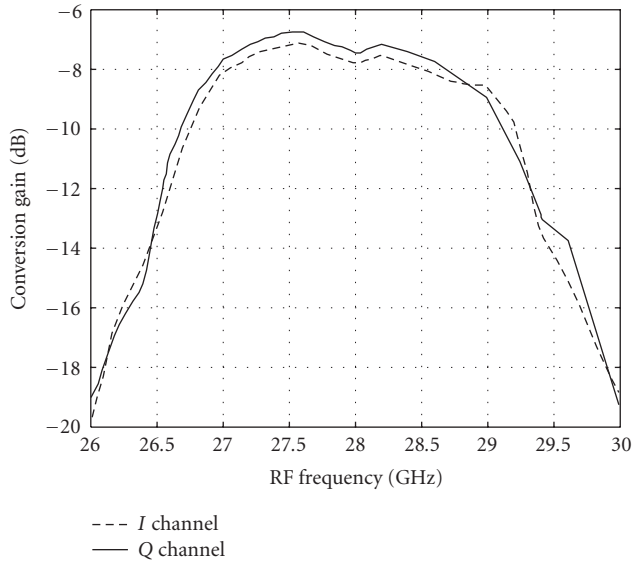

Figure 12: Conversion gain versus RF frequency for I and Q channels at LO power of 10 dBm.

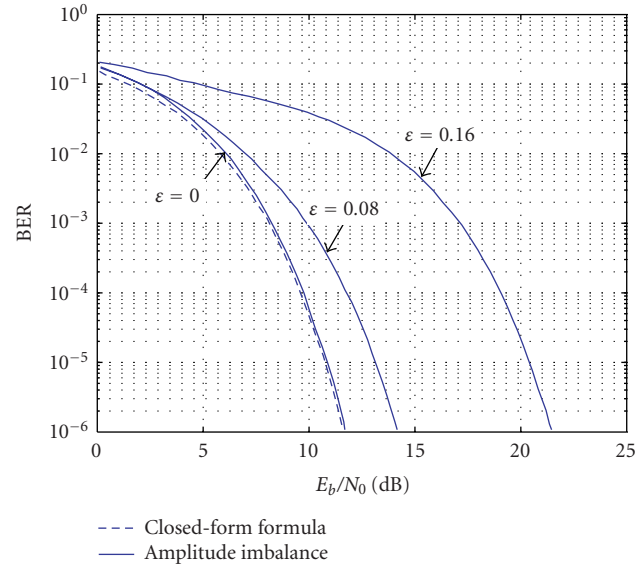

Figure 13: BER of the 16 QAM signal versus E_b/N_0 as a function of ε. From left to right $\varepsilon = 0, 0.08, 0.16$. Dashed line represents BER calculated-from the closed form formula.

equal to

$$\widetilde{I} = 2\alpha i_s \sqrt{\frac{2E_{\min}}{T_s}} I_2\left(\alpha\left(1+\frac{\varepsilon}{2}\right)\right)[a_i\cos\theta - b_i\sin\theta],$$
$$\widetilde{Q} = 2\alpha i_s \sqrt{\frac{2E_{\min}}{T_s}} I_2\left(\alpha\left(1-\frac{\varepsilon}{2}\right)\right)[b_i\cos\theta - a_i\sin\theta]. \quad (9)$$

It can be seen that in either case, the errors in the nominally 45° phase shifts and mismatches between the amplitudes of the I and Q signal corrupt the downconverted signal constellation, thereby rising the bit error rate. In continue, we calculate the BER for different levels of amplitude and phase imbalances. For this purpose, we use the signal space concepts described in [11]. We derive algorithms to do this calculations for 16, 64, and 256-QAM schemes. We also use approximate-closed-form formula in (10) to compare our results with

$$\text{BER} = \frac{4}{\log_2 M}\left(1-\frac{1}{\sqrt{M}}\right)Q\left(\sqrt{\frac{3(Eb/N0)\log_2 M}{(M-1)}}\right). \quad (10)$$

First, we assume amplitude imbalance. Figure 13 shows the BER of the 16-QAM signal for ε values of 0, 0.08, 0.16. It also illustrates the BER obtained from closed-form formula that is in agreement with our result for $\varepsilon = 0$. From the figure, it can be seen that as the amplitude error increases, the amount of Eb/N0 required to have BER of 10e-6 increases. In 16-QAM modulation, if the amplitude error in I and Q paths reaches 28 percent, the BER will be irreducible. This error for 64 and 265-QAM is 11 and 5 percent, respectively. Figure 14 illustrates BER of 16, 64, and 256-QAM schemes in permitted ranges of amplitude error. In continue, we consider phase errors. Like amplitude error, as phase error increases the amount of Eb/N0 required to have BER of 10e-6 increases. In 16-QAM modulation, if phase error in I and Q paths reaches 20 degree, the BER will be irreducible. This error for 64 and 256-QAM is 9 and 4 degrees, respectively. Figure 15 shows BER of 16, 64, and 256-QAM schemes in permitted ranges of phase error. So, in M-ary QAM, as M increases, the amount of permitted amplitude and phase errors reduces and the amount of BER increases.

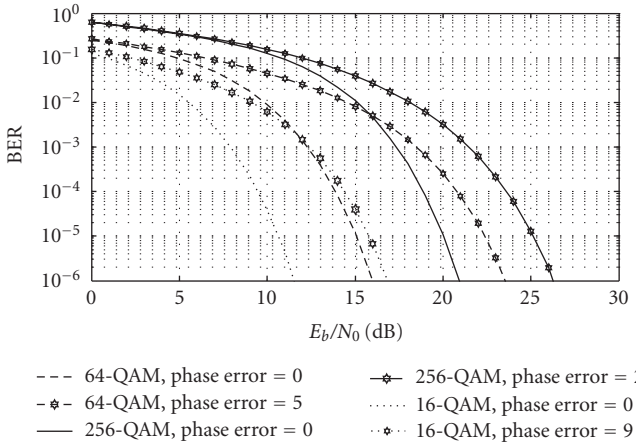

Figure 14: BER versus E_b/N_0 for 16, 64, 256-QAM in permitted ranges of amplitude error. From left to right: 16-QAM: $\varepsilon = 0, 0.12$, 64-QAM: $\varepsilon = 0, 0.03$, 256-QAM: $\varepsilon = 0, 0.014$.

5.2. BER calculations in presence of DC offsets

The unbalance effects in APDP created by mismatch in the IV characteristics of diodes causes DC offsets. If saturation currents i_s and slope parameters α are different for the two

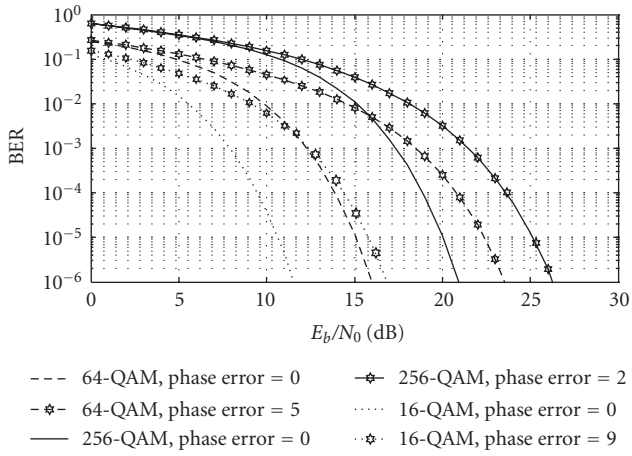

FIGURE 15: BER versus E_b/N_0 for 16, 64, 256-QAM in permitted ranges of phase error. From left to right: 16-QAM: $\theta = 0, 9$ degrees, 64-QAM: $\theta = 0, 5$ degrees, 256-QAM: $\theta = 0, 2$ degrees.

diodes of the APDP, we may assume that

$$\begin{aligned} i_{s1} &= i_s + \Delta i_s, \qquad i_{s2} = i_s - \Delta i_s, \\ \alpha_1 &= \alpha + \Delta\alpha, \qquad \alpha_2 = \alpha - \Delta\alpha. \end{aligned} \tag{11}$$

As we know from [4], the conductance expressions for i_s and α mismatches can be, respectively, written as follows:

$$\begin{aligned} g_{\Delta i_s} &= 2\alpha i_s \left[\cosh \alpha V + \frac{\Delta i_s}{i_s} \sinh \alpha V \right], \\ g_{\Delta\alpha} &= 2\alpha i_s e^{(\Delta\alpha)V} \left[\cosh \alpha V + \frac{\Delta\alpha}{\alpha} \sinh \alpha V \right]. \end{aligned} \tag{12}$$

Like in the previous section, we multiply these conductances to the applied voltage. The output current of the APDP has a DC offset that is equal to

$$\begin{aligned} i_{\text{dc-offset}} = {} & 2\alpha i_s V_{\text{Lo}} I_1(\Delta\alpha V_{\text{Lo}}) \times \left[I_0(\alpha V_{\text{Lo}}) + I_2(\alpha V_{\text{Lo}}) \right] \\ & \pm 2\alpha(\Delta i_s) V_{\text{Lo}} I_1(\alpha V_{\text{Lo}}). \end{aligned} \tag{13}$$

Current terms add constructively when one of the diodes has both a higher slope and higher saturation current. They add destructively otherwise. So the output currents in I and Q paths after a lowpass filter are equal to

$$\begin{aligned} \widetilde{I} &= 2\alpha i_s \sqrt{\frac{2E_{\min}}{T_s}} I_2(\alpha V_{\text{Lo}}) a_i + i_{\text{dc-offset}}, \\ \widetilde{Q} &= 2\alpha i_s \sqrt{\frac{2E_{\min}}{T_s}} I_2(\alpha V_{\text{Lo}}) b_i + i_{\text{dc-offset}}. \end{aligned} \tag{14}$$

$\Delta\alpha$ and Δi_s may be different in I and Q paths. So, the signal constellation is corrupted and the BER increases. In continue, we calculate the BER due to different levels of diode imbalances. As the mismatches increase, the amount of Eb/N0 required to have BER of 10e-6 increases. For example, in 16-QAM signal, we consider different cases of mismatch

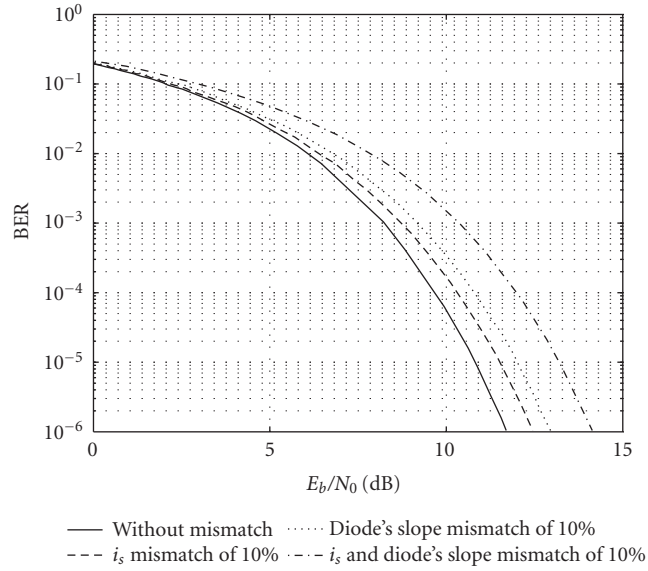

FIGURE 16: BER of 16-QAM signal for different levels of diodes mismatches. From left to right: without mismatch, i_s mismatch of 10%, α mismatch of 10%, both α and i_s mismatch of 10%.

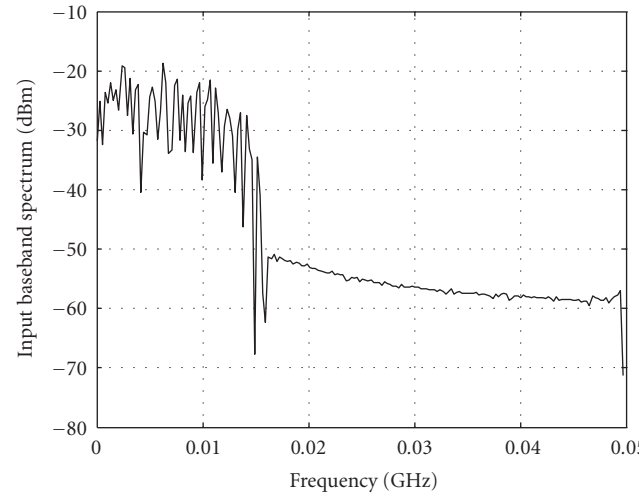

FIGURE 17: Input baseband signal spectrum.

that are shown in Figure 16. It can be seen that the effect of α mismatch on BER degradation is more than i_s mismatch [12].

6. COMMUNICATION LINK FOR 16-QAM SIGNAL

A communication link is constructed with the proposed modulator-demodulator. The link is simulated with baseband I and Q signals corresponding to 16-QAM modulation format with data rate 110 Mbps. We set the LO power to 10 dBm and its frequency to 14 GHz. Spectral response of input baseband signals is shown in Figure 17. Then, the modulated signal at the RF port of the modulator is sent to the demodulator input. The RF modulated signal spectrum

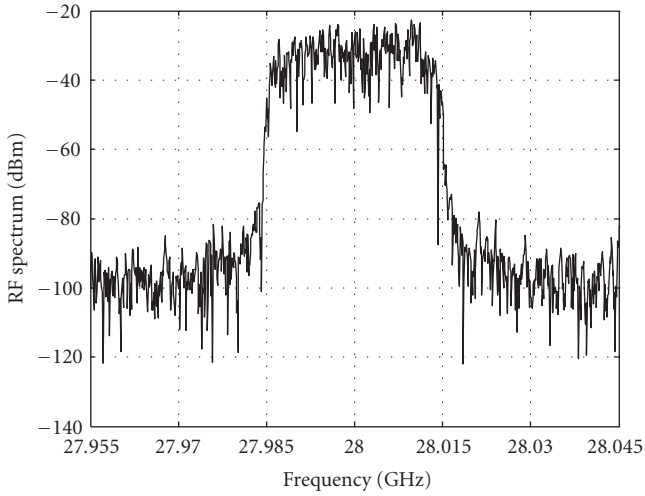

Figure 18: Output spectrum of the modulator at 28 GHz.

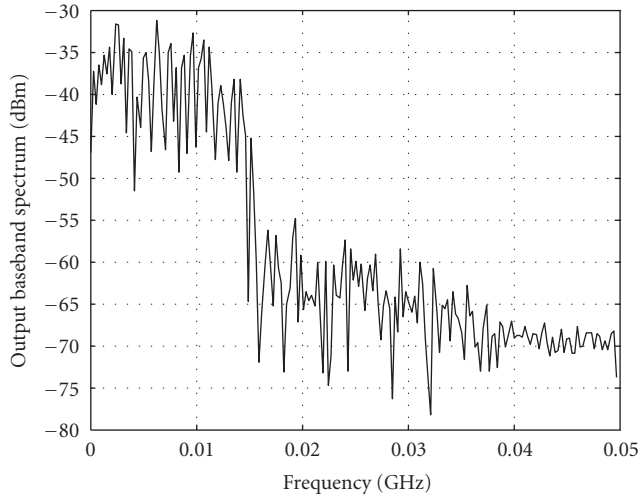

Figure 19: Output demodulated signal spectrum.

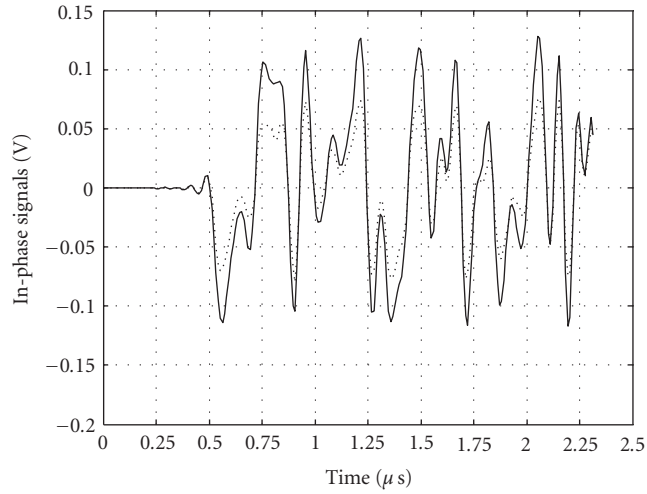

Figure 20: Input and output in-phase signals.

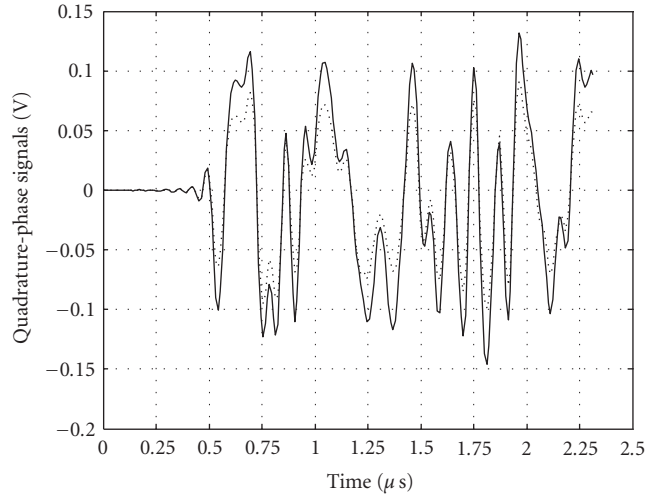

Figure 21: Input and output quadrature-phase signals.

is depicted in Figure 18. As can be seen from this figure, the data rate of the system is 110 Mbps. Finally, the RF-modulated signal is demodulated with the LO signal. The output baseband signals are produced at the land demodulator's I and Q ports. Spectral response of these signals is drawn in Figure 19. As may be seen, the proposed structure efficiently transmits the modulated signal. In-phase and quadrature-phase signals at time domain are presented in Figures 20 and 21. The figures show a close agreement between input and output signals at time domain both in I and Q paths.

7. CONCLUSION

Direct conversion circuitry with even harmonic mixers based on antiparallel diode pair (APDP) was used to realize a Ka band even harmonic quadrature modulator-demodulator operating at 28 GHz. Self-biased APDP was used in order to flatten the conversion loss of the system versus LO power. The system structure is very attractive, because of reducing hardware complexity and cost. The impacts of I/Q imbalances and DC offsets on BER performance of the system was also considered. A communication link is built with the proposed modulator-demodulator. The experimental results show that this system can be a low-cost and high-performance 16-QAM transceiver for LMDS applications.

ACKNOWLEDGMENTS

The authors wish to thank the editor and the anonymous reviewers for their insightful comments and suggestions which greatly improved the presentation of this work. This work was supported in part by Iran Telecommunication Research Center (ITRC) and the Academic Research Section of Iran Management and Planning Organization (#102) under Contract 1721.

REFERENCES

[1] M. Cohn, J. E. Degenford, and B. A. Newman, "Harmonic mixing with an antiparallel diode pair," *IEEE Transactions on Microwave Theory and Techniques*, vol. 23, no. 8, pp. 667–673, 1975.

[2] K. Itoh, A. Iida, Y. Sasaki, and S. Urasaki, "A 40 GHz band monolithic even harmonic mixer with an antiparallel diode pair," in *Proceedings of IEEE MTT-S International Microwave Symposium Digest*, vol. 2, pp. 879–882, Boston, Mass, USA, June 1991.

[3] M. R. Barber, "Noise figure and conversion loss of the schottky barrier diode," *IEEE Transactions on Microwave Theory and Techniques*, vol. 15, no. 11, pp. 629–635, 1967.

[4] C. J. Verver, D. Drolet, M. G. Stubbs, and C. Pike, "Development of a Ka-band even harmonic modulator for a satellite briefcase terminal," in *Proceedings of Asia Pacific Microwave Conference (APMC '99)*, vol. 2, pp. 448–451, Singapore, November-December 1999.

[5] M. W. Chapman and S. Raman, "A 60 GHz uniplanar MMIC 4X subharmonic mixer," in *Proceedings of IEEE MTT-S International Microwave Symposium Digest*, vol. 3, pp. 95–98, Phoenix, Ariz, USA, May 2001.

[6] M. Shimozawa, T. Katsura, K. Maeda, et al., "An even harmonic mixer using self-biased anti-parallel diode pair," in *Proceedings of IEEE MTT-S International Microwave Symposium Digest*, vol. 1, pp. 253–256, Seattle, Wash, USA, June 2002.

[7] P. Blount and C. Trantanella, "A high IP3, subharmonically pumped mixer for LMDS applications," in *Proceedings of the 22nd Annual Gallium Arsenide Integrated Circuit (GaAs IC '00)*, pp. 171–174, Seattle, Wash, USA, November 2000.

[8] J.-Y. Park, S.-S. Jeon, Y. Wang, and T. Itoh, "Integrated antenna with direct conversion circuitry for broad-band millimeter-wave communications," *IEEE Transactions on Microwave Theory and Techniques*, vol. 51, no. 5, pp. 1482–1488, 2003.

[9] I. Telliez, A.-M. Couturier, C. Rumelhard, C. Versnaeyen, P. Champion, and D. Fayol, "A compact, monolithic microwave demodulator-modulator for 64-QAM digital radio links," *IEEE Transactions on Microwave Theory and Techniques*, vol. 39, no. 12, pp. 1947–1954, 1991.

[10] P. J. Lee, "Computation of the bit error rate of coherent m-ary psk with gray code bit mapping," *IEEE Transactions on Communications*, vol. 34, no. 5, pp. 488–491, 1986.

[11] L. Jianhua, K. B. Letaief, J. C.-I. Chuang, and M. L. Liou, "M-PSK and M-QAM BER computation using signal-space concepts," *IEEE Transactions on Communications*, vol. 47, no. 2, pp. 181–184, 1999.

[12] F. Shayegh, A. Mohammadi, and A. Abdipour, "Characterization of EHM direct conversion transceivers in Ka-band," in *Proceedings of the 35th European Microwave Conference (EUMC '05)*, pp. 371–374, Paris, France, October 2005.